Journal of Hydrology 590 (2020) 125537

Contents lists available at ScienceDirect

Journal of Hydrology

journal homepage: www.elsevier.com/locate/jhydrol

Research papers

Hydrogeological characteristics of groundwater and surface water associated with two small lake systems on King George Island, Antarctica

Jisun Kim[a], Sung-Wook Jeen[a,b,*], Hyoun Soo Lim[c], Jeonghoon Lee[d], Ok-Sun Kim[e], Hyoungseok Lee[e], Soon Gyu Hong[e]

[a] Department of Environment and Energy, Jeonbuk National University, Jeonju, Republic of Korea
[b] Department of Earth and Environmental Sciences & The Earth and Environmental Science System Research Center, Jeonbuk National University, Jeonju, Republic of Korea
[c] Department of Geological Sciences, Pusan National University, Busan, Republic of Korea
[d] Deptartment of Science Education, Ewha Womans University, Seoul, Republic of Korea
[e] Korea Polar Research Institute (KOPRI), Incheon, Republic of Korea

ARTICLE INFO

This manuscript was handled by Huaming Guo, Editor-in-Chief

Keywords:
Water cycle
Antarctica
Lake
Hydraulic conductivity
Groundwater flux
Isotope

ABSTRACT

Although groundwater is an important component of the water cycle in the polar regions, groundwater in Antarctica has rarely been studied. This study evaluated the physical and chemical characteristics of groundwater, surface water, and snow in two lakes on the Barton Peninsula, King George Island, Antarctica, with a particular focus on groundwater. Influxes/outfluxes of groundwater were measured using seepage meters, and hydraulic conductivities were calculated based on grain size analysis for the sediments. A total of 41 water samples were used to determine the chemical compositions and isotopic ratios of oxygen and hydrogen. The groundwater fluxes measured in one lake (referred to as "Lake A") were $-9.9 \times 10^{-10} \sim 2.7 \times 10^{-9}$ m/s (average of $-9.1 \times 10^{-10} \pm 3.6 \times 10^{-9}$ m/s) and in a second lake (referred to as "Lake B") were $2.2 \times 10^{-9} \sim 3.0 \times 10^{-9}$ m/s (average of $2.6 \times 10^{-9} \pm 4.0 \times 10^{-10}$ m/s). This indicates that groundwater flux is highly dynamic in Lake A, whereas groundwater influx in Lake B is relatively stable. Hydraulic conductivity for the lake sediments ranged between 1.7×10^{-6} m/s and 2.1×10^{-4} m/s. Oxygen and hydrogen isotopic compositions followed the global meteoric water line (GMWL) and local meteoric water line (LMWL), indicating that groundwater and surface water in the study area originate from the atmosphere. Evaporation may not be an influential factor probably due to the relatively humid climate during the summer season in the study area. Groundwater and surface water might partially experience isotopic exchange fractionation during and after the snow melting process. The chemical composition of groundwater was distinguished from that of surface water and snow by higher concentrations of major anions (Cl, SO_4, and alkalinity), major cations (Ca, Mg, K, and Na), and trace elements (Si, Li, Sr, Mn, Zn, and Cu), resulting from water-rock interactions. To the best of our knowledge, this is the first study to directly measure groundwater fluxes in lake systems in Antarctica, and to evaluate the characteristics of groundwater in the Barton Peninsula. It may therefore serve as a basis for studying the role of groundwater in the water cycle of Antarctica.

1. Introduction

Groundwater is the third most abundant component of the global water cycle, following the oceans and snow/glaciers. Groundwater and snow/glaciers together account for more than 97% of total fresh water on Earth (Healy and Scanlon, 2010). As such, groundwater constitutes a very important part of the global water cycle; in spite of this, its importance has largely been overlooked, particularly in the polar regions. Recently, there has been growing concern that climate change may rapidly and irrevocably alter global ecosystems (Schiedek et al., 2007). In particular, the Antarctic environment is highly sensitive to global warming because of its extreme weather conditions (Knap et al., 1996). According to the Intergovernmental Panel on Climate Change (IPCC) report (IPCC, 2001), the climate of Antarctica has become wetter and warmer in recent decades. Moreover, in permafrost regions climatic changes may lead to changes in the depth of the active layer, which

* Corresponding author at: Department of Earth and Environmental Sciences & The Earth and Environmental Science System Research Center, Jeonbuk National University, Jeonju, Republic of Korea.
E-mail address: sjeen@jbnu.ac.kr (S.-W. Jeen).

https://doi.org/10.1016/j.jhydrol.2020.125537
Received 4 June 2020; Received in revised form 8 September 2020; Accepted 9 September 2020
Available online 14 September 2020

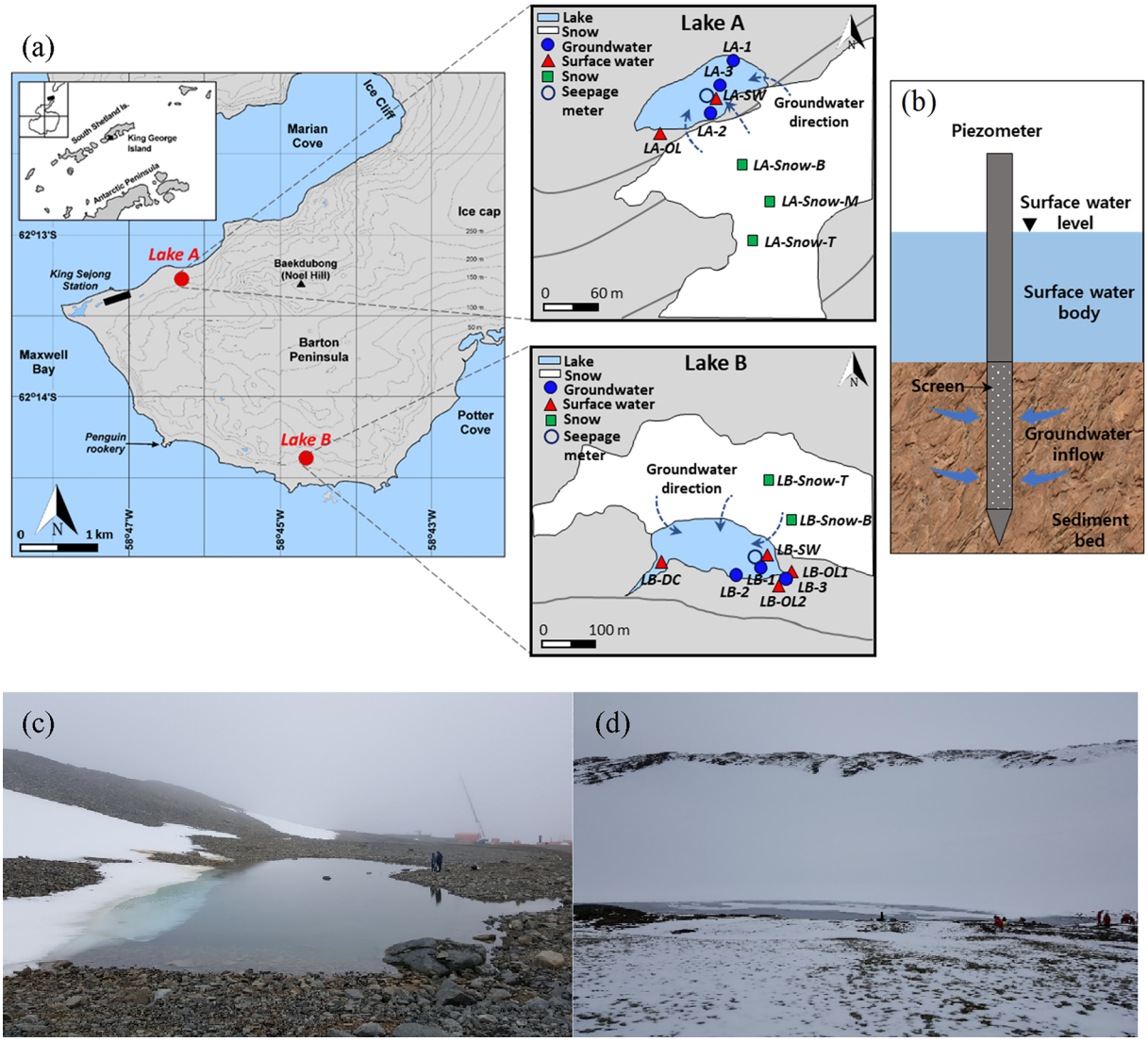

Fig. 1. (a) Locations of the two lakes near King Sejong Station in Antarctica, with map showing detailed sampling locations for Lake A and Lake B. On the map, LA-1, LA-2, LA-3, LB-1, LB-2, and LB-3 (LA: Lake A, LB: Lake B) represent groundwater samples, SW and OL represent lake water (surface water) and overland flow samples, respectively, and LA-snow and LB-snow represent snow samples; the subscripts T, M, and B for the snow samples represent top, middle, and bottom samples with respect to the elevation of the mountain slope. The open blue circle indicates the location of seepage meter, and the blue dotted arrows represent the estimated groundwater flow directions. (b) Schematic diagram of the piezometer. Actual photographs of (c) Lake A and (d) Lake B are also shown. (For interpretation of the references to colour in this figure legend, the reader is referred to the web version of this article.)

may alter the flow path of groundwater. The changes in groundwater flow systems may alter interactions between surface water and groundwater, and it can ultimately lead to changes in the water cycle of the polar regions (Quinton et al., 2011). To understand changes in the water cycle in the polar regions as a result of climate change, it is therefore essential to study interactions between groundwater, surface water, and snow/glacier. However, studies on the water cycle have rarely included groundwater, which forms an important part of the water balance in the polar regions.

In recent decades, a growing number of studies on changes in the glacial and sea-ice coverage of Antarctica have been conducted (Ducklow et al., 2007; Ross et al., 1996; Smith et al., 1995). It has also been suggested that change in the rate of submarine groundwater discharge is a factor affecting fluctuations in sea level as a result of climate change; studies of groundwater have pointed to its role in regulating sea-level change. Sawagaki and Hirakawa (2002) indicated that interconnected subglacial lakes in Antarctica may enable rapid water migration, eventually discharging into the ocean. Wingham et al. (2006) also suggested that subglacial lakes and their interconnected drainage systems can affect the mechanisms associated with water flow in Antarctica. Uemura et al. (2011) indicated direct submarine groundwater discharge in Lützow-Holm Bay, Antarctica. They suggested that the volumes of the groundwater contributions from the continent to the ocean may be significant, and thus it is necessary not only to estimate the mass balance of glaciers, but also to measure the water flow of submarine groundwater directly. Moreover, in a study by Hofstee et al. (2006), the extent, duration and chemical properties of groundwater were characterized, and tracer tests were conducted to estimate groundwater velocity in Seabee Hook, Cape Hallett, Antarctica. Although highly informative, these studies are insufficient to provide a comprehensive picture on groundwater dynamics in Antarctica from the water cycle point of view.

Barton Peninsula is located in the southwest region of King George Island, the largest of the South Shetland Islands, at the northwest tip of the Antarctic Peninsula. King George Island has a series of ice-free peninsulas, hosting a complex network of interlinked lakes and rivers fed by glaciers, snow, and rain, underlain by a thick permafrost (Headland, 1984). Polar research stations have been established by various

countries throughout King George Island. The King Sejong Station, which is managed by the Korea Polar Research Institute (KOPRI), has been operating continuously since it was established in 1988. Since then, it has been a site for research in a variety of fields, including geology, oceanography, seismology, glaciology, climatology, and ecology. Past research related specifically to water regimes near King Sejong Station include studies of heavy metal content in seawater (Ahn et al., 1996), precipitation variations related to El Niño (Kwon and Lee, 2002), analyses of isotope variation in fresh water (Kim et al., 2008) and seawater (Khim et al., 1997), and studies of glaciers (Kim et al., 2015; Park et al., 1998). More recently, the influence of sea salt on fresh water has been evaluated by analyzing the water quality of meltwater and pondwater in coastal regions of Antarctica (Lim et al., 2014). The temperatures of soil, meltwater ponds, and seawater have been analyzed to evaluate the thermal characteristics of soil and water, using time-series analyses (Lee et al., 2016). Lee et al. (2020) have also evaluated the isotopic characterization of snow/ice and its meltwater on King George Island. To date, however, there has been no study that focuses on the hydrogeological and chemical characteristics of groundwater in the Barton Peninsula.

This study investigated interactions between groundwater, surface water, and snow in two small lakes near the King Sejong Station, by evaluating groundwater influx and outflux, the hydraulic conductivity of lake sediments, and the chemical and the isotopic composition of groundwater, surface water, and snow. To the best of our knowledge, it is the first study to directly measure groundwater flux in lake systems in Antarctica, and the chemical and isotopic composition of groundwater in the Barton Peninsula. Its findings may thus serve as a basis for evaluating the role of groundwater in the water cycle of Antarctica.

2. Study area

Located between S61°50′ to S62°15′ and W57°30′ to W59°01′, King George Island is the largest volcanic island in the South Shetland Islands archipelago (Lee et al., 2020). The study area is located in a coastal region of the Barton Peninsula (Fig. 1), where King Sejong Station (Korean Antarctic Research Station) (S62°13′ and W58°47′) has been operating since 1988 (Lee et al., 2016). King George Island has a surface area of around 1310 km^2, of which more than 92% is covered by glaciers (Lim et al., 2014). Dominated by an oceanic climate, it is relatively warm and humid compared to the Antarctic Peninsula (Kim et al., 2007). According to weather data for 2018 from the automatic meteorological observation system (AMOS) at King Sejong Station, average air pressure is 988.0 hPa (highest 1024 hPa, lowest 948 hPa), average air temperature is −1.8℃ (maximum 9.7℃, minimum −20.2℃), average wind speed is 7.8 m/s (gust 37.3 m/s, northerly), average relative humidity is 86.2%, and total annual precipitation is 363.0 mm (a monthly average of 33.0 mm).

Barton Peninsula is geologically composed of volcaniclastic sedimentary rocks (the Sejong Formation), calc-alkaline volcanic, and intrusive rocks (Yoo et al., 2001). The Sejong Formation forms the lowest stratigraphic unit and is of Eocene age (Yoo et al., 2001). It is largely composed of subaerial volcaniclastic sediments such as agglomerate, tuff breccia, and lapilli tuff, with a maximum thickness of 200 m, and is distributed along the southern and southwestern coasts of the Barton Peninsula (Chun et al., 1994; Yoo et al., 2001). Fossil leaves in fine-grained Sejong sandstones are suggestive of Late Paleocene to Eocene age (Chun et al., 1994). Above the Sejong Formation, mafic to intermediate volcanic rocks are widespread in the Baton Peninsula; they consist mostly of basaltic andesite containing plagioclase or pyroxene phenocrysts and are associated with massive andesite (Yeo et al., 2004). The central northwestern area of the Barton Peninsula includes a very small mass of fine-crystalline diorite and a relatively large stock of medium-crystalline granodiorite (Lee et al., 2019). The ice-free area of the peninsula is of gentle topography, with a wide central plain lying at 90–180 m above sea level (Lee et al., 2019). Bedrocks in the ice-free areas are mostly covered by glacial till. The peninsula's active layer has a depth of approximately 1 m, with an underlying permafrost layer (Lee et al., 2004).

This study was conducted at two small lakes on the Barton Peninsula (Fig. 1). The first of these (referred to as "Lake A"; S62°13 '22.2", W58°46'50.0") is located approximately 0.5 km from King Sejong Station, in the coastal area near Marian Cove. The mountain slope on which it is located has a light scattering of snow with occasional no snow cover during the summer season, and its sedimentary layer consists of rocky sediments. The second lake (referred to as "Lake B"; S62°14 '23.4", W58 °44 '36.2") is located on the KGL01 site (S62°14 '24", W58 °44 '36", at an altitude of 39 m), an eco-physiological research site of the KOPRI (Cho et al., 2020), in the coastal area in the vicinity of Maxwell Bay. Around 90% of the surface area of the mountain slope behind Lake B is covered with snow, whose meltwater is a source of the lake water. A variety of lichens and moss species are also distributed around Lake B, which are supplied with water from the snow meltwater and precipitation (Cho et al., 2020). Water from direct precipitation and/or snow meltwater from the mountain slope enters the lakes mainly as overland flow and groundwater flow. The water influx appears to be highly related to the amount of snow melt which is associated with air temperature and perhaps the changes in depths of the active layer. Groundwater appears to flow at shallow depths through the active layer and to partially be converted to interflow and overland flow while travelling to the lake. The estimated groundwater flow directions are indicated as the blue dotted lines in Fig. 1a. There is no distinct discharge point in Lake A whereas the lake water in Lake B is discharged through a small creek located at the downgradient of the lake (LB-DC; Fig. 1a). The relative size of each lake varies according to the prevailing meltwater and weather conditions; as a guideline, at one-time point (in March 2016), Lake A was 64 m long and 25 m wide, while Lake B was 94 m long and 26 m wide. The depth of Lake A changed dynamically between 0 and approximately 1.5 m, and the maximum depth of Lake B was estimated to be approximately 3 to 5 m.

3. Methods

3.1. Sediment sampling and analysis

A total of 9 sediment samples were collected for grain size analysis and mineral identification during the summer season of 2018 (January 2018). Among these, 4 samples were collected from Lake A and 5 from Lake B. Sediment samples were collected from the bed of each lake, near points where seepage meters were installed. Collected samples were shipped frozen for further analysis.

For grain size analysis, a typical sieve analysis was conducted for all sediment samples, and SediGraph analysis was used for micro-particle analysis. For sieve analysis, samples were dried naturally in the indoor laboratory prior to sieving. Approximately 200 g of each dried sample was mounted on a sieve shaker and shaken for 10 min, using sieve screen sizes of 2 mm, 1 mm, 0.5 mm, 0.25 mm, 0.125 mm, and 0.063 mm. The masses of the different particle size classes were then measured and their mass percentages computed.

For SediGraph analysis, samples were dried in a vacuum with a temperature of −80℃ for 2–3 days in a forced convection drying oven (HB-502 M, Hanbeak Scientific Co., Korea). The proportion with grain size larger than 63 μm (e.g., sand and gravel) was classified through wet sieving, while for the proportion with size smaller than 63 μm (e.g., clay and silk) a micro-measurement SediGraph III 5100 (Micromeritics Instruments Co., USA) was used for micro-particle analysis. Grain size analysis using SediGraph III 5100 was performed at the Department of Geological Sciences of Pusan National University, Korea.

Using the results of grain size analysis, the hydraulic conductivity of the sediments was calculated. This can be estimated by the relationship between sediment porosity and particle diameter. For the purposes of this study, hydraulic conductivity was calculated using the empirical

formula suggested by Vukovic and Soro (1992), as follows:

$$K = \frac{g}{v} \bullet C \bullet f(n) \bullet d_e^2 \quad (1)$$

where K is the hydraulic conductivity [L T^{-1}], g is the acceleration due to gravity [L T^{-2}], v is the 20 °C standard kinematic viscosity [L^2 T^{-1}], C is the sorting coefficient (dimensionless), $f(n)$ is the porosity function (dimensionless), and d_e is the effective grain diameter [L]. The kinematic viscosity (v) is related to the dynamic viscosity and the fluid (water) density, as follows:

$$v = \frac{\mu}{\rho} \quad (2)$$

where μ is the dynamic viscosity [M L^{-1} T^{-1}] and ρ is the density [M L^{-3}] of the fluid. The porosity (n) (dimensionless) can be derived from the empirical relationship with the coefficient of grain uniformity (U), as follows:

$$n = 0.255(1 + 0.83^U) \quad (3)$$

where U is the coefficient of grain uniformity (dimensionless), expressed as follows:

$$U = \left(\frac{d_{60}}{d_{10}}\right) \quad (4)$$

where d_{60} and d_{10} are the grain diameter [L] of the soil particles, corresponding to 60% and 10% of the passing weight percentage in the particle size distribution curve which is known as the effective grain diameter. Previous studies have presented the empirical formulae with various C, $f(n)$, and d_e values and domains of applicability, although they take the general form presented in equation (1) above. These empirical formulae, summarized by Odong (2013), are shown in Table 1.

To identify minerals in the sediment samples, a multi-purpose high-performance X-ray diffractometer (XRD) was used. The analysis was performed with an X'pert pro powder (PANalytical Co., Netherlands) device located at the Center for University-Wide Research Facilities of Jeonbuk National University; operating conditions were an acceleration voltage of 40 kV and an applied current of 30 mA. The Inorganic Crystal Structure Database (ICSD) (Flz Karlsruhe, Germany) was used to identify the crystal phase of minerals.

3.2. Measuring water flux between groundwater and surface water

A seepage meter was used for direct measurement of groundwater flux (Lee and Cherry, 1979). The meter is a cylinder that is open at the base and vented at the top, and is embedded in the lake's sedimentary layer, enclosing the sediment-surface water interface. A plastic collection bag containing a given volume of water is connected to the vent on the top of the meter, after which the volume change in the water remaining in the collection bag after a measured time period is monitored. The flux of water measured indicates the amount and direction of water flowing across the boundary between groundwater and surface water. In this study, positive values indicate flow from groundwater to surface water, while negative values indicate flow from surface water to the aquifer. Seepage flux velocities (Q_v) were calculated using the following equation:

$$Q_v = (V_f - V_0)/At \quad (5)$$

where V_0 is the initial volume of water contained in the collection bag [L^3], V_f is the volume of water remaining after a measured period of time [L^3], t is the time elapsed from installation of the collection bag to its removal [T], and A is the cross-sectional area of the seepage meter [L], in other words the area of the deposition layer covered by the seepage meter [L^2]. In this way, the water flux in the seepage meter is expressed as a unit of velocity (volume per unit area per unit time) [L T^{-1}].

In this study, a custom-built seepage meter with a diameter of 700 mm and a height of 200 mm was used (Fig. 2). One seepage meter each was installed in Lake A and Lake B, embedded in the sediment of each lake with as tight a seal as possible. A few small rocks on the lake bottom were removed during the installation, and it was ensured that the seepage meters are securely installed into the lake sediment by stepping on them. Over a given period of time, the change of water volume flowing into and out of the collection bag was measured. The volume change was divided by the cross-sectional area of the seepage meter and the elapsed time, giving the groundwater influx/outflux per unit surface area. During the study period, water fluxes were measured a total of 7 times for Lake A and 3 times for Lake B. The time intervals for the measurement were approximately one day for Lake A and 5 to 6 days for Lake B. Measurement for Lake B was particularly limited due to accessibility (approximately 5 km walking distance) and unfavorable weather conditions. On several occasions, the collection bag was found in torn condition, probably due to attacks by skuas (predatory seabirds). For the measure of lake level, a stick was installed in the lake sediment and it was used as a reference point. Lake level was measured manually on the same day of the flux measurement.

3.3. Water sampling and analysis

In total, 41 water samples were collected from both lakes. They were classified as groundwater, surface water, or snow, depending on the type of water. The number of samples for each water type were 14, 16, and 11, for groundwater, surface water, and snow, respectively. The groundwater samples were obtained from piezometers installed on the bed and the boundary of each lake (Fig. 1). The piezometers consisted of a stainless steel pipe 133 cm in length with an internal diameter of 2.1 cm. A screen was located from 10 cm to 33 cm from the lower tip. They were installed to a depth of around 40 cm below the lake bed so that the entire screen section was embedded in the sediment. Plastic tubing and Waterra pumps (Waterra Co., Luxembourg) were used to collect groundwater samples from the piezometers. Groundwater samples were taken after purging at least three pore volumes of stagnant water inside each piezometer. Surface water (lake water) was collected

Table 1
Empirical formulae used to estimate hydraulic conductivity in this study.

Source	C [a]	$f(n)$ [b]	d_e [c]	Remark
Hazen (1892)	6.0×10^{-4}	$[1 + 10(n\text{-}0.26)]$	d_{10}	$U < 5$, 0.1 mm $< d_{10} <$ 3.0 mm[1, 2]
Kozeny-Carman (Carman, (1956)	8.3×10^{-3}	$[n^3/(1\text{-}n)^2]$	d_{10}	$d_{10} <$ 3.0 mm, Medium sand[3]
Beyer (1966)	6.0×10^{-4}	$\log(500/U)$	d_{10}	$1 < U < 20$, 0.06 mm $< d_{10} <$ 0.6 mm[1, 2]
Terzaghi (1925)	$6.1 \times 10^{-3} \sim 10.7 \times 10^{-3}$	$(\text{n-}0.13/3\sqrt[3]{1-n})^2$	d_{10}	C = 8.4x10^{-3}, Large-grain sand[4]
Slichter (1898)	1.0×10^{-2}	$n^{3.287}$	d_{10}	0.01 mm $< d_{10} <$ 5.0 mm[1, 2]
USBR (United States Bureau of Reclamation) (Bialas, 1966)	4.8×10^{-4}	$d_{20}{}^{0.3}$	d_{20}	$U < 5$, Medium-grain sand[4]

References: [1] Kasenow (2002), [2] Odong (2013), [3] Carrier (2003), [4] Cheng and Chen (2007).
[a] Sorting coefficient (dimensionless).
[b] Porosity function (dimensionless).
[c] Effective grain diameter (in mm).

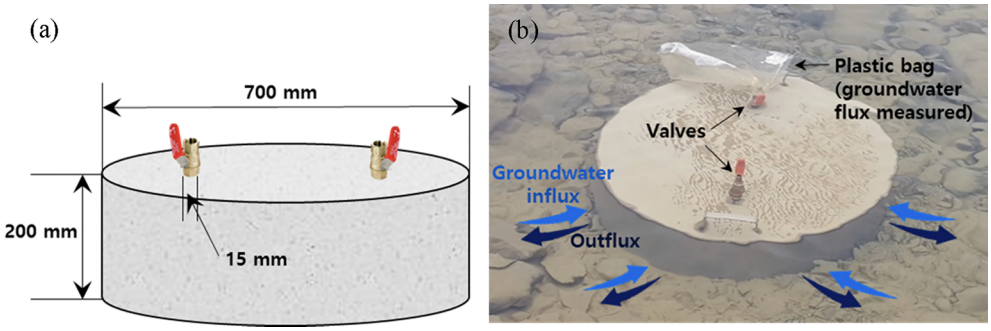

Fig. 2. (a) Schematic diagram and (b) real picture of seepage meter installed on lake bed. The locations for the seepage meters installed at each lake are indicated by the blue open circle in Fig. 1a. (For interpretation of the references to colour in this figure legend, the reader is referred to the web version of this article.)

Table 2
Results of grain size analysis.

Sampling site[a]	Sample name	Composition (wt%)[b]				Texture parameter [c]		Sediment
		Gravel	Sand	Silt	Clay	Mean	Sorting	type[d]
LA	LA-1	51.48	28.67	10.70	9.14	Coarse sand	Poorly sorted	msG
	LA-2	41.76	41.76	7.77	8.71	Coarse sand	Poorly sorted	msG
	LA-3(1/2)	0	53.94	29.03	17.03	Coarse silt	Poorly sorted	mS
	LA-3(2/2)	0	52.04	29.51	18.45	Coarse silt	Poorly sorted	mS
	Average	23.31	44.10	19.25	13.33	Fine sand	Poorly sorted	gmS
	SD[e]	27.21	11.60	11.63	5.13	–	–	–
LB	LB-1(1/4)	49.83	47.35	1.31	1.51	Very coarse sand	Moderately well sorted	sG
	LB-1(2/4)	46.05	51.82	0.39	1.75	Very coarse sand	Moderately well sorted	sG
	LB-1(3/4)	47.49	42.02	3.16	7.33	Coarse sand	Poorly sorted	msG
	LB-1(4/4)	35.05	54.51	3.0	7.44	Coarse sand	Poorly sorted	msG
	LB-2	32.26	51.40	6.17	10.16	Medium sand	Poorly sorted	msG
	Average	42.14	49.42	2.81	5.64	Coarse sand	Poorly sorted	msG
	SD[e].	17.82	12.10	2.34	5.12	–	–	–

[a] LA: Lake A, LB: Lake B.
[b] Weight percentage (%): gravel (> 2 mm), sand (0.063–2 mm), silt (0.004–0.063 mm), and clay (< 0.004 mm) (Wentworth, 1922).
[c] Mean and sorting were calculated using the equations of Folk and Ward (1957).
[d] Sediment type: msG: muddy sand gravel, mS: muddy sand, sG: sand gravel, and gmS: gravel muddy sand (Folk, 1954).
[e] Standard deviation.

Table 3
Hydraulic conductivity calculated from grain size analysis using the empirical formulae presented in Table 1.

Sampling site[a]	Sample name	d_e[b]			n[c]	U[d]	Hydraulic conductivity (m/s)					
		d_{10}	D_{20}	d_{60}			Hazen (1892)	Carman (1956)	Beyer (1966)	Terzaghi (1925)	Slichter (1898)	Bialas (1966)
LA	LA-1	0.04[e]	0.08	2.1	0.26	52.50	8.9×10^{-6}	3.9×10^{-6}	9.1×10^{-6}	2.5×10^{-6}	1.7×10^{-6}	1.4×10^{-5}
	LA-2	0.06	0.16	2.15	0.26	34.13	2.2×10^{-5}	9.6×10^{-6}	2.7×10^{-5}	6.2×10^{-6}	4.3×10^{-6}	6.9×10^{-5}
	LA-3 (1/2)	NA	0.01	0.04	NA	NA	NA	NA	NA	NA	NA	NA
	LA-3 (2/2)	NA	0.002	0.05	NA	NA	NA	NA	NA	NA	NA	NA
	Average[f]	0.05	0.12	2.13	0.26	43.31	1.5×10^{-5}	6.7×10^{-6}	1.8×10^{-5}	4.3×10^{-6}	3.0×10^{-6}	4.1×10^{-5}
LB	LB-1 (1/4)	0.14	0.26	1.80	0.28	13.33	1.2×10^{-4}	5.9×10^{-5}	1.7×10^{-4}	3.9×10^{-5}	2.6×10^{-5}	2.1×10^{-4}
	LB-1 (2/4)	0.15	0.25	1.32	0.30	8.92	1.8×10^{-4}	1.0×10^{-4}	2.2×10^{-4}	6.8×10^{-5}	4.2×10^{-5}	1.9×10^{-4}
	LB-1 (3/4)	0.06	0.09	0.56	0.30	8.89	3.3×10^{-5}	1.8×10^{-5}	4.0×10^{-5}	1.2×10^{-5}	7.7×10^{-6}	1.6×10^{-5}
	LB-1 (4/4)	0.07	0.09	0.71	0.29	10.85	3.2×10^{-5}	1.6×10^{-5}	4.1×10^{-5}	1.1×10^{-5}	6.9×10^{-6}	1.8×10^{-5}
	LB-2	0.052[e]	0.07	0.35	0.33	6.73[e]	2.6×10^{-5}	1.7×10^{-5}	2.9×10^{-5}	1.1×10^{-5}	6.7×10^{-6}	1.0×10^{-5}
	Average	0.09	0.15	0.95	0.30	9.74	8.0×10^{-5}	4.2×10^{-5}	1.0×10^{-4}	2.8×10^{-5}	1.8×10^{-5}	8.9×10^{-5}
	SD[g]	0.05	0.10	0.60	0.02	2.48	7.0×10^{-5}	3.8×10^{-5}	8.9×10^{-5}	2.5×10^{-5}	1.6×10^{-5}	1.0×10^{-4}

[a] LA: Lake A, LB: Lake B.
[b] Effective grain diameter (in mm).
[c] Porosity (dimensionless).
[d] Coefficient of grain uniformity (dimensionless).
[e] Estimated.
[f] LA-3 (1/2) and LA-3 (2/2) were excluded.
[g] Standard deviation
NA: Not applicable; measurement of the effective grain diameter (d_{10}) is not applicable because the cumulative percentage of soil with size less than the minimum grain size that can be measured by the SediGraph is greater than 10%.

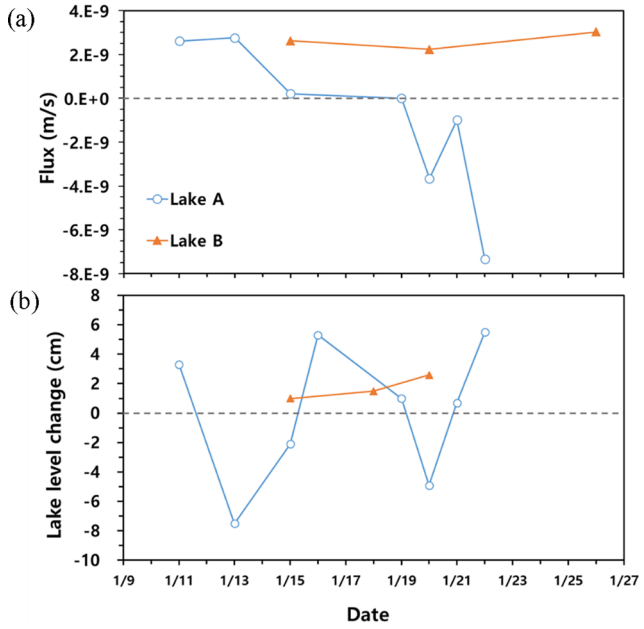

Fig. 3. (a) Groundwater flux and (b) changes in water level measured in Lake A and Lake B. The gray horizontal dotted lines represent the zero flux and no lake level change, respectively.

at a depth of around 30 cm from each lake's surface. Overland flow, which was flowing at the inlet of the lake, was also classified as surface water. In the case of snow samples from Lake A, samples were collected at the lower, middle, and upper locations of the mountain slope, depending on altitude. In the event of fresh snowfall, new samples were collected from the same sites used for collecting previous ones. Snow samples from Lake B were collected at the lower and upper locations of the mountain slope. Sampling locations for groundwater, surface water, and snow are shown in Fig. 1.

For analysis of water quality, temperature, pH, oxidation-reduction potential (ORP), dissolved oxygen (DO), and electrical conductivity (EC) were measured *in situ* immediately after water sampling. Alkalinity analysis of the samples was performed at the indoor laboratory of King Sejong Station on the same day as sampling, after filtering with a 0.45 μm syringe filter by titration with 0.16 N sulfuric acid (H_2SO_4) using a digital titrator (Hach Co., USA). All other samples for cation, anion, and isotope analyses were also filtered with 0.45 μm syringe filters. For cation samples, ultra-pure nitric acid (HNO_3) (Sigma-Aldrich, USA) was added to each water sample to reduce the solution pH level to below 2. All samples were shipped frozen to the laboratory in Korea for further analysis. All water samples were collected in high-density polyethylene (HDPE) bottles without head space and frozen immediately after sampling. Analyses were conducted immediately after thawing the frozen samples in the laboratory. Cation analysis was conducted using an inductively coupled plasma mass spectrometer (ICP-MS; iCAP RQ, Thermo Fisher Scientific, USA) at the Center for University-Wide Research Facilities at Jeonbuk National University. Anions were analyzed by an ion chromatograph (ICS-90; Thermo Fisher Scientific, USA) and Chromeleon™ software (Thermo Fisher Scientific, USA) in the Department of Earth and Environmental Sciences at Jeonbuk National University.

Oxygen and hydrogen isotopic composition was analyzed at the KOPRI (Incheon, Korea) with an L1102-i isotopic water liquid analyzer (Picarro Inc., Sunnyvale, CA, USA) using the wavelength-scanned cavity ring-down spectroscopy (WS-CRDS) principle (Jung et al., 2013). The international measurement standards used were the Second Vienna Standard Mean Ocean Water (VSMOW2) ($\delta^{18}O$: 0‰, δD: 0‰), the Greenland Ice Sheet Project (GISP) ($\delta^{18}O$: −24.76‰, δD: − 189.5‰), and the second Standard Light Antarctic Precipitation (SLAP2) ($\delta^{18}O$: −55.50‰, δD: −427.5‰) provided by the International Atomic Energy Agency (IAEA) for normalization of δ scale for oxygen isotope ratios (Kim et al., 2019). The standard deviation of $\delta^{18}O$ ranged from 0.05‰ to 0.06‰, while that of δ^2H ranged from 0.31‰ to 0.36‰. The margin of error using the $\delta^{18}O$ and δ^2H average values for each sample was ± 0.1‰ for $\delta^{18}O$ and ± 1‰ for δ^2H, based on the values analyzed by isotope ratio mass spectrometry (IRMS) (Jung et al., 2013).

4. Results and discussion

4.1. Physical and chemical properties of sediment

4.1.1. Grain size analysis

The results of grain size analysis for the Lake A and Lake B sediments analyzed by SediGraph are shown in Table 2. The grain sizes of the sediments were classified as gravel (> 2 mm), sand (0.063–2 mm), silt (0.004–0.063 mm), and clay (< 0.004 mm), in accordance with the grain size scale of Wentworth (1922). Mean grain size and sorting were calculated using the equations suggested by Folk and Ward (1957). Sediment types were classified based on percentages of gravel, sand, silt, and mud (Folk, 1954).

The sediment samples collected from the lower (LA-1) and upper (LA-2) parts of Lake A (Fig. 1) were predominantly composed of gravel (42–52%) and sand (29–42%). The mean grain size and sorting were classified as poorly sorted coarse sand and muddy sand gravel types, respectively. By contrast, one sample collected from the center of Lake A (LA-3) contained 0% gravel, with sand as the predominant size (54–54%). This sample was classified as the poorly sorted coarse silt and muddy sand types. On average, the mean grain size of Lake A belonged to the fine sand type, while the sediment was poorly sorted and belonged to the gravel muddy sand type.

In the case of Lake B, a sample from the up-gradient of the lake (LB-1) contained relatively little silt (0.4–3.2%) and clay (1.5–7.4%). The sample was also determined to contain relatively high amounts of organic materials. LB-2, a sample collected from the lower area of Lake B, had the highest contents of silt and clay among the samples from Lake B. It was classified as poorly sorted medium sand and, and its sediment as muddy sand gravel. On average, Lake B consisted of poorly sorted coarse sand and was classified as muddy sand gravel.

It was shown that grain size and sediment sorting differ even in the same lake, and may vary according to the mineral composition and weathering of the original rocks. It is likely that differences in bedrock geology affect physical and chemical weathering processes in the Antarctic region, and that transport and deposit processes determine different soil and sediment features (Malandrino et al., 2009). The coarser sediment at a shallower depth (e.g., near shoreline) is probably due to greater depositional energy than that for the sediment at a deeper depth (e.g., center of the lake), which has finer grain size. Comparing the two lakes, the sediment of Lake A showed higher percentages of silt and clay than Lake B. The grain size analysis thus suggests that Lake A may be more restricted to groundwater flow than Lake B due to the former's higher silt and clay content. However, it should be noted that the samples collected in this study may represent only parts of the lakes.

4.1.2. Hydraulic conductivity determined from grain size analysis

The hydraulic conductivity (K) of the sediment samples was determined using the empirical formulae presented in Table 1. Nine samples were collected from Lake A and Lake B, but of these only seven were used for calculation because the effective grain diameter could not be determined for the remaining two samples (LA-3 (1/2) and LA-3 (2/2)).

Table 3 summarizes the hydraulic conductivity values for each sample using the empirical formulae presented in Table 1. For Lake A, the values for LA-1 ranged between 1.7×10^{-6} m/s and 1.4×10^{-5}

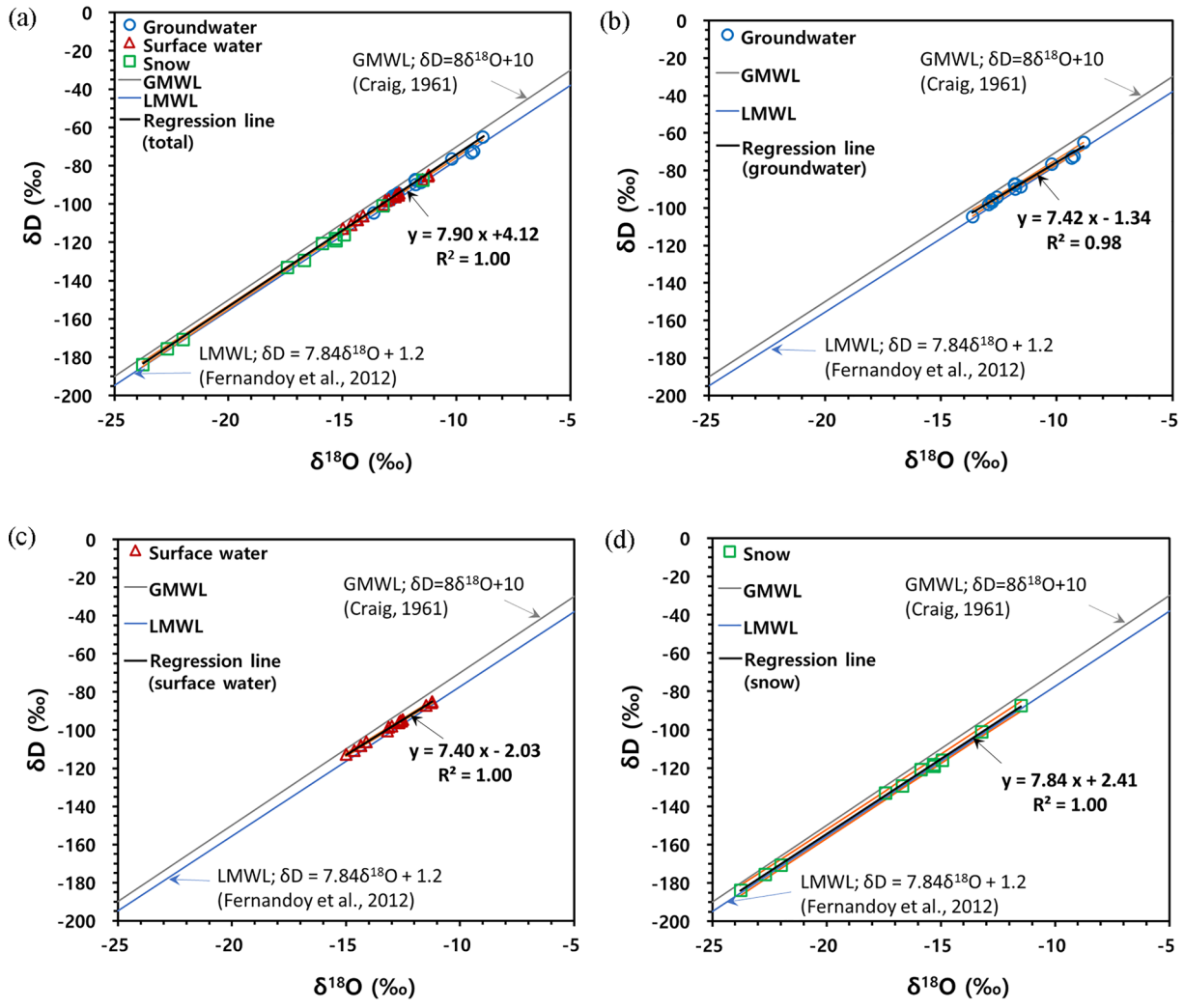

Fig. 4. (a) Oxygen and hydrogen isotopic composition of groundwater, surface water, and snow in Lake A and Lake B, along with the regression line for all water samples. GMWL (the black dotted line) represents the global meteoric water line (Craig, 1961; $\delta D = 8\delta^{18}O + 10$) and LMWL (the blue dotted line) represents the local meteoric water line (Fernandoy et al., 2012; $\delta D = 7.84\delta^{18}O + 1.2$). The orange dotted lines indicate the 95% confidence intervals of the regression line (Note that the region between the upper and lower lines for (c) are narrow). Individual oxygen and hydrogen isotopic composition and regression lines for (b) groundwater, (c) surface water, and (d) snow in Lake A and Lake B are also shown. (For interpretation of the references to colour in this figure legend, the reader is referred to the web version of this article.)

m/s, while for LA-2 they ranged between 4.3 × 10^{-6} m/s and 6.9 × 10^{-5} m/s. For Lake B, the values for LB-1 ranged between 6.9 × 10^{-6} m/s and 2.1 × 10^{-4} m/s, and those for LB-2 ranged between 6.7 × 10^{-6} m/s and 1.0 × 10^{-5} m/s. The relatively lower hydraulic conductivity of Lake A compared to Lake B (Table 3) can be attributed to its relatively large fine sand and poorly sorted soil content (Table 2). Mean grain size and sorting were thus closely related to hydraulic conductivity (Shepherd, 1989). Comparing hydraulic conductivity values calculated using different empirical formulae, these varied by roughly one order of magnitude. The lowest value was calculated based on Slichter (1898) and the highest was based on Bialas (1966) (Vukovic and Soro, 1992).

The hydraulic conductivity range for typical glacial outwash is from 10^{-5} to 10^{-3} m/s (Fetter, 1994). The hydraulic conductivity measured in active layer soils in the McMurdo Dry Valleys, Antarctica, using the pressure head difference and steady-state flow rate, ranged from 1.6 × 10^{-6} to 6.2 × 10^{-3} m/s (Schmidt and Levy, 2017). Thus, both the range of hydraulic conductivity values and the dependence of hydraulic conductivity on sediment sorting in this study is generally consistent with the study of Schmidt and Levy (2017), which showed that hydraulic conductivity is higher in well-sorted than poorly-sorted soils. Overall, the hydraulic conductivity measured in this study is a contribution to the very small quantity of existing data on hydraulic conductivity in ice-free regions of Antarctica (Levy, 2012; Levy et al., 2011).

4.1.3. Mineralogical composition

An XRD analysis of the sediments of Lake A identified the presence of plagioclases (andesine [$(Ca,Na)(Al,Si)_4O_8$] and anorthite [$CaAl_2Si_2O_8$]), quartz [SiO_2], and pyroxenes (clinopyroxene [$Ca(Mg,Fe)(SiO_3)_2$] and orthopyroxene [$(Mg,Fe)SiO_3$]). In Lake B, quartz, pyroxene, and andesine, as well as feldspar [$(K,Na,Ca)(Al,Si)_4O_8$] were identified.

According to Jeong and Yoon (2001), the areas where the two lakes are located are mainly composed of basaltic and andesitic tuff/lava. The plagioclase content for the Lake A and Lake B areas was 60–80% and 80%, respectively. The quartz content of the Lake A and Lake B areas was 10–15% and 5–15%, respectively (Jeong and Yoon, 2001). Jeong et al. (2004) have shown that plagioclase and quartz respectively account for an average of 61% and 15% of mineralogical composition throughout the Barton Peninsula. In the areas where our study sites are located, relatively minor amounts of pyroxene, amphibole, laumontite,

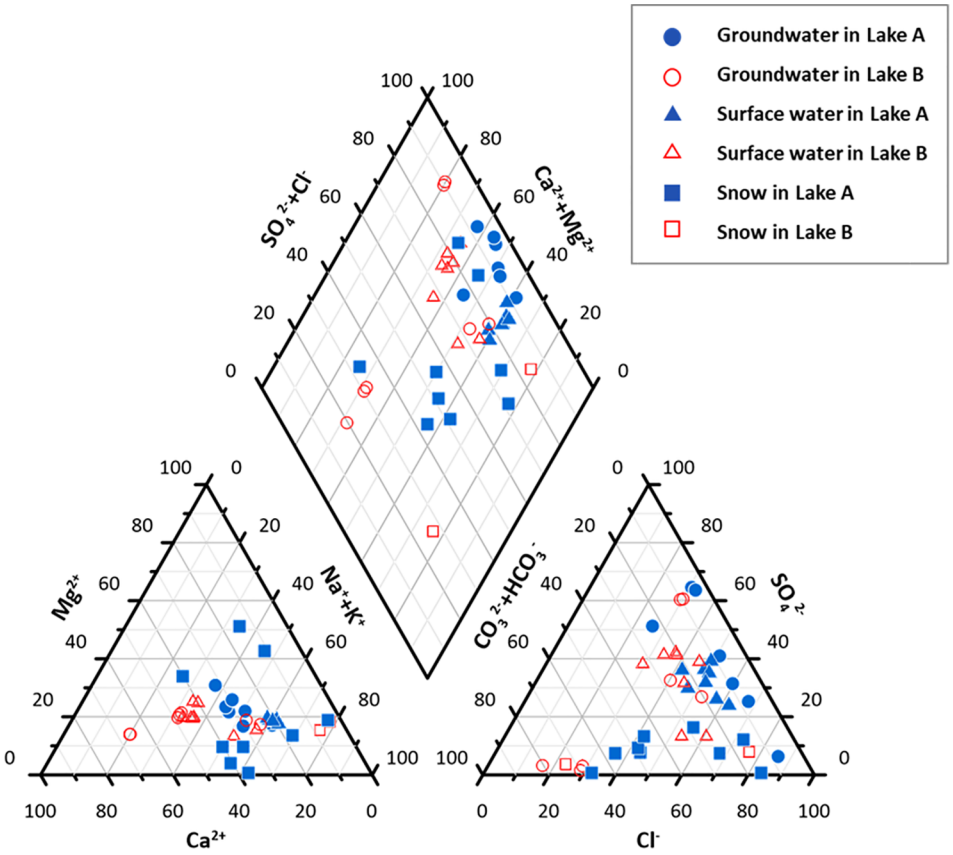

Fig. 5. Piper diagram for composition of groundwater, surface water, and snow in Lake A and Lake B.

calcite, pyrite, and pyrophyllite were also detected. In addition, images of thin sections revealed the presence of quartz, calcic plagioclase, sodic plagioclase, K-feldspar, amphibole, pyroxene, volcanic glass, and diatom fragments (Jeong et al., 2004).

The mineral composition of the two lakes, identified by XRD analysis in this study, is thus generally consistent with the bedrock lithology of the Barton Peninsula reported in previous studies, showing that plagioclase and pyroxene were derived from basaltic and andesitic tuff/lava (Jeong et al., 2004). Quartz is derived from devitrification of volcanic glass to chlorite and quartz, and directly from granitoids that are also sources for other minerals, including amphiboles, plagioclase, and micas (Jeong and Yoon, 2001).

The mineralogical information from the XRD analysis indicates that major cations in groundwater, including calcium, magnesium, sodium, potassium, aluminum, iron, and silicon, can originate from water-rock interactions during shallow groundwater flow in the active layer. Certain characteristics of groundwater chemistry, to be discussed later, show that water-rock interactions may be a determining factor for the chemical composition of groundwater in this Antarctic region, as they also are elsewhere in the world.

4.2. Fluxes of groundwater

The groundwater fluxes per unit area measured in the two lakes are shown in Fig. 3a. Positive values indicate that the flow is from groundwater into surface water, while negative values of groundwater flux indicate outflux from surface water to groundwater. Despite the short measurement period for the study, both influx and outflux were observed at the same location in Lake A: influx of 2.0×10^{-10} m/s ~ 2.7×10^{-9} m/s (from groundwater to surface water) and outflux of -9.9×10^{-10} m/s ~ -7.3×10^{-9} m/s (from surface water to groundwater) were measured, showing that the groundwater fluxes in Lake A are highly dynamic (average of $-9.1 \times 10^{-10} \pm 3.6 \times 10^{-9}$ m/s). In Lake B, by contrast, only influx of 2.2×10^{-9} m/s ~ 3.0×10^{-9} m/s (average of $2.6 \times 10^{-9} \pm 4.0 \times 10^{-10}$ m/s) was observed, indicating that the lake is likely a more stable system whose water is consistently supplied by groundwater. A longer observational period would be required to confirm this.

The magnitude of groundwater fluxes in the two lakes was not fully consistent with the hydraulic conductivity values for the lake sediments calculated from the grain size analysis. This may be partly due to the variety of available formulae and heterogeneity and uncertainty in calculations of hydraulic conductivity. Moreover, using only a single seepage meter to measure groundwater flux in each lake may not be representative of flux in the lake as a whole. Leaving aside the uncertainty and heterogeneity associated with the hydraulic conductivities of the lake sediments, the differences in the pattern and magnitude of groundwater flux between Lake A and Lake B may be largely attributable to topography and temporal and spatial differences in hydraulic gradient between surface water and groundwater. Measuring spatio-temporal changes in hydraulic heads for groundwater and surface water warrants further investigation. Increasing the number of measuring points is also essential to enhance the representativeness of data on groundwater influx and outflux. Monitoring should be conducted for a longer time period to have a better understanding of the lake systems.

Fig. 3b shows fluctuations in water level of the two lakes. In the case of Lake A, the dynamic changes both in water level and lake size (not shown, but observed visually during the investigation period) indicate that it is a highly dynamic system. However, groundwater flux (Fig. 3a) did not correlate directly to changes in water level changes, probably because the water level was constantly responding to new precipitation and snow meltwater being added to the lake. The non-correlation between groundwater flux and water level may also be related to changes

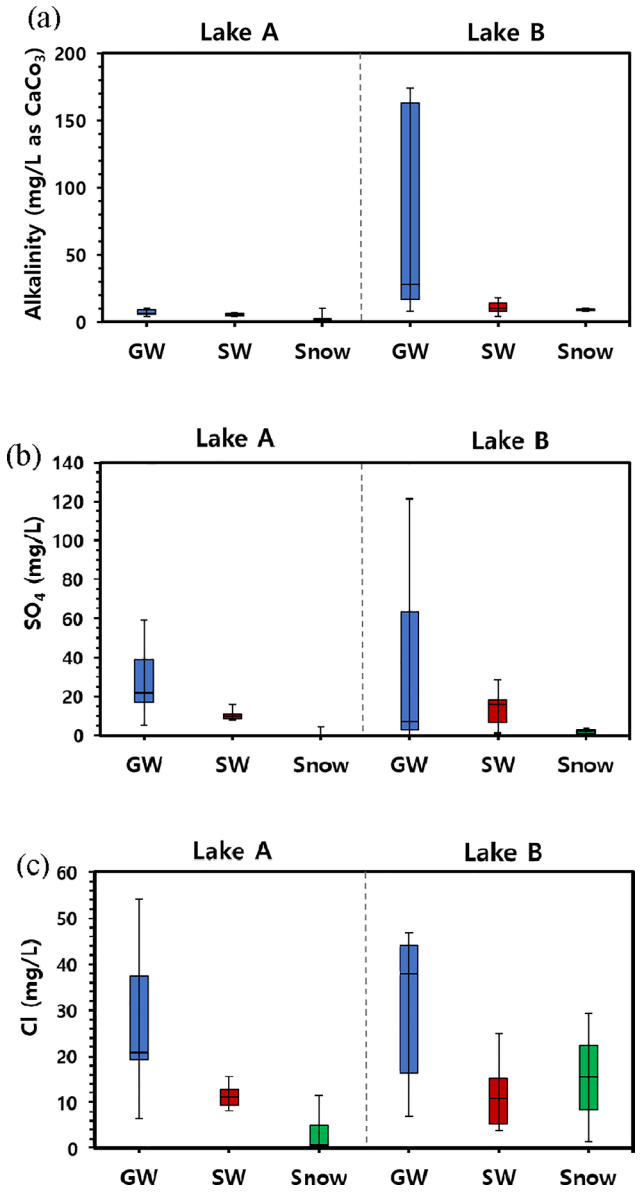

Fig. 6. Box and whisker plots showing distribution of anions ((a) alkalinity, (b) SO_4, and (c) Cl) in groundwater, surface water and snow of Lake A and Lake B. In the box plot, the center line represents the median, while the upper and lower lines represent the 75th and 25th percentiles, respectively. The upper and lower whiskers represent the maximum and minimum, respectively.

in the thickness of the active layer. By contrast, water level and lake size in Lake B corresponded closely with groundwater influx (Fig. 3a and b), indicating that it is a stable lake system. This is further confirmed by the presence of a stable ecosystem of lichens and moss species around Lake B, in contrast to Lake A. It can thus be inferred that in addition to snow meltwater, groundwater is a significant source of water and is one of the important factors in maintaining lake ecosystems such as Lake B in this Antarctic region.

4.3. Characteristics of groundwater, surface water, and snow

4.3.1. Oxygen and hydrogen isotopic composition

Table S1 shows the oxygen and hydrogen isotopic compositions of groundwater, surface water, and snow in the two lakes. The $\delta^{18}O$ and δD of groundwater in Lake A and Lake B showed a range of −13.63 to −8.85‰ and −104.6 to −64.9‰, respectively, while those of surface water showed a range of −14.99 to −9.78‰ and −112.8 to −77.4‰, respectively. For each lake, the $\delta^{18}O$ and δD of snow showed a range of −23.78 to −11.50‰ and −183.7 to −87.4‰, respectively. Fig. 4 shows $\delta^{18}O$ and δD of groundwater, surface water, and snow in both lakes. For comparison, both the global meteoric water line (GMWL) (Craig, 1961; $\delta D = 8\delta^{18}O + 10$) and the local meteoric water line (LMWL) were plotted. The LMWL for precipitation samples for the nearby O'Higgins Station defined by Fernandoy et al. (2012) was $\delta D = 7.84\delta^{18}O + 1.2$.

Regression line for all water samples was $\delta D = 7.90 (\pm 0.06)\delta^{18}O + 4.12 (\pm 0.89)$ ($n = 41$, $r^2 = 0.9975$), while regression lines for groundwater, surface water, and snow were $\delta D = 7.42 (\pm 0.30)\delta^{18}O - 1.32 (\pm 3.53)$ ($n = 14$, $r^2 = 0.9802$), $\delta D = 7.40 (\pm 0.08)\delta^{18}O - 2.03 (\pm 1.15)$ ($n = 16$, $r^2 = 0.998$), and $\delta D = 7.84 (\pm 0.08)\delta^{18}O - 2.41 (\pm 1.41)$ ($n = 11$, $r^2 = 0.9991$), respectively. The regression line slope for snow was similar to those of the GMWL and LMWL, while those for surface water and groundwater deviated slightly from those of the GMWL and LMWL. The regression slope defined by Simões et al. (2004) for the ice cores in King George Island was $\delta D = 7.1\delta^{18}O - 2.2$. Lim et al. (2014) showed that the regression lines for meltwater and pondwater on the Barton Peninsula were $\delta D = 7.23\delta^{18}O - 4.26$ and $\delta D = 7.76\delta^{18}O - 0.72$, respectively. Recently, Lee et al. (2020) showed that the slope of the $\delta^{18}O$ and δD relationship for snow and its meltwater over the Barton Peninsula was $\delta D = 7.0\delta^{18}O - 5.9$. This indicates that the melting process may cause isotopic fractionation.

The snow of Lake A and Lake B does not generally appear to have undergone evaporation, due to the relatively humid climate during the summer season in the study area. In the case of water that has undergone isotope exchange between solid ice or snow and liquid water, the slope is 6.3 (Lee et al., 2009). The slopes for the groundwater and surface water of the two lakes were higher than this slope. This may suggest that the melted water from snow partially underwent isotopic exchange reactions and then was further infiltrated into groundwater and/or flowed to surface water.

4.3.2. Field geochemical parameters

The chemical composition of groundwater, surface water, and snow in the two lakes is summarized in Table S2. In both lakes, the pH of groundwater was not substantially different from that of surface water: in Lake A, the average pH values of groundwater and surface water were 5.23 and 5.53, respectively, while in Lake B, they were 6.73 and 7.20, respectively. The relatively low pH values in groundwater and surface water in Lake A may represent the low pH buffering capacities of waters. The EC of groundwater in both lakes was higher than that of surface water: in Lake A, the average EC values of groundwater and surface water were 197 and 104 μS/cm, respectively, while in Lake B, they were 528 and 129 μS/cm, respectively. Notably, the EC of Lake B's groundwater was more than twice that of Lake A. This may be due to slower groundwater velocity in Lake B compared to Lake A, thus providing longer residence time for water-rock interaction. On the other hand, in Lake A, groundwater may be partially mixed with surface water, as indicated by the measured groundwater fluxes (Fig. 3a).

The DOs of groundwater and surface water in Lake A did not differ significantly, showing average values of 10.0 and 12.10 mg/L, respectively. The groundwater and surface water of Lake B showed average values of 4.33 and 10.61 mg/L, respectively. This indicates that groundwater and surface water in Lake A are similar to each other in terms of redox chemistry, whereas Lake B's groundwater is under more reduced conditions compared to those of its surface water. These results are also consistent with the Eh values. In Lake A, the average Eh both for groundwater and surface water was not substantially different, with the values of 539 and 536 mV, respectively. In Lake B, the Eh values of groundwater and surface water showed that groundwater is under relatively reduced conditions compared to surface water, with the average values of 277 and 442 mV, respectively. Notably, the LB-1 groundwater sample showed the lowest DO (< 1.38 mg/L) and Eh

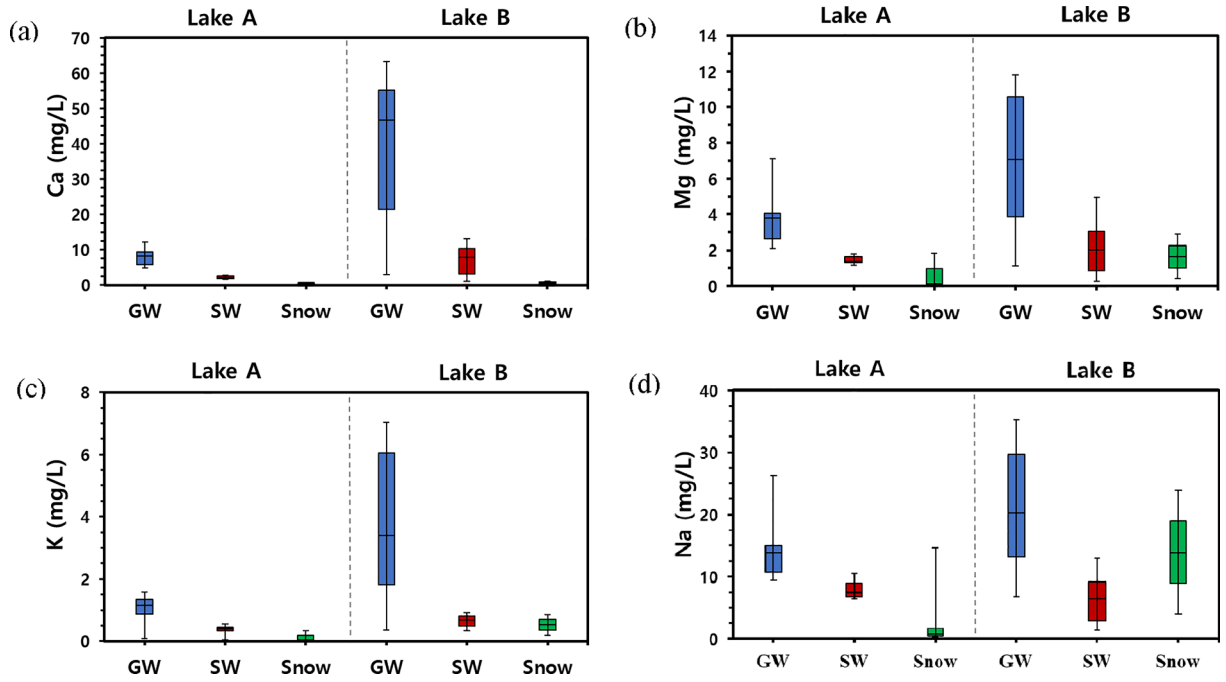

Fig. 7. Box and whisker plots showing distribution of major cations ((a) Ca, (b) Mg, (c) K, and (d) Na) in groundwater, surface water and snow of Lake A and Lake B. In the box plot, the center line represents the median, while the upper and lower lines represent the 75th and 25th percentiles, respectively. The upper and lower whiskers represent the maximum and minimum, respectively.

(< 175 mV) values compared to those of the other groundwater samples. The sediment collected at this sampling point (LB-1 sediment sample) contained organic-rich materials that originated as debris from dead lichens and mosses. This suggests that the lake sediment at the study site may also reflect locally heterogeneous geochemical conditions.

The average alkalinity values of groundwater and surface water in Lake A were 7 and 5 mg/L as $CaCO_3$, respectively, while in Lake B they were 81 and 11 mg/L as $CaCO_3$, respectively. The alkalinity of Lake B's groundwater was thus around 12 times higher than that of Lake A, suggesting that HCO_3^- in Lake B's groundwater may be derived from the decomposition of organic materials. In a typical oxidation-reduction environment in groundwater, organic substrates such as dead mosses can be used as energy and carbon sources for bacterial metabolism consuming dissolved oxygen and generating bicarbonate (Appelo et al., 2005). In Lake B, mosses are widely distributed along the shoreline, providing a source of organic materials on the lake bed after they die. By contrast, Lake A consists only of rocky sediment, without the presence of mosses. Overall, the field water quality parameters both for groundwater and surface water in Lake A were not substantially different, whereas in Lake B they differed considerably.

4.3.3. Water chemistry of major and trace elements

The chemical composition of major cations and anions for all water samples was plotted in a Piper diagram (Fig. 5). The groundwater in this study was classified as Ca-HCO_3 type and Ca-Na-SO_4-Cl type. Ca-HCO_3 is a typical water type of fresh water found in volcanic rock areas (Lim et al., 2014), while Ca-Na-SO_4-Cl type may indicate mixing of various sources, such as water-rock interaction or the influence of sea salt. Surface water was classified as Ca-Na-SO_4-Cl type for both lakes. A previous study of meltwater and pondwater on the Barton Peninsula (Lim et al., 2014) has shown that surface water in the area can be classified as Ca-Cl type, which is partially affected by sea salt and water-rock interaction. The surface water in this study generally showed higher Na and SO_4 concentrations than in the earlier study. While in Lake A groundwater and surface water showed similar chemical compositions, Lake B's groundwater composition was more varied, including Ca-HCO_3 and Ca-Na-SO_4-Cl types. Lake B's groundwater composition may thus indicate longer groundwater flow paths from the recharge to the discharge area. The water composition of snow mainly belonged to the Ca-Na-Cl and Na-Cl types, suggesting the influence of sea salt spray; during storms, breaking waves and high winds may carry large volumes of seawater spray considerable distances inland (Hofstee et al., 2006).

Variations in alkalinity, SO_4, and Cl in the groundwater, surface water, and snow of the two lakes are presented in box and whisker plots (Fig. 6). The concentrations of alkalinity, SO_4, and Cl in groundwater were relatively higher than those of surface water and snow. The very high alkalinity of Lake B may be due to the decomposition of organic-rich materials, as discussed above. The concentration of SO_4 in Lake B's groundwater was also higher than for that of Lake A. This may suggest more water-rock interaction, such as the alteration of sulfide minerals (Lim et al., 2014). Cl concentrations in groundwater and snow of Lake B were higher than those in surface water. This may suggest that the melted snow affected by sea salt spray infiltrates into groundwater and experiences water-rock interactions after infiltration. In general, both groundwater and surface water in Lake A are similar in composition, whereas in Lake B their composition is significantly different. This may indicate more dynamic mixing between surface water and groundwater in Lake A, which is supported by the measured groundwater flux and water level changes.

Fig. 7 shows differences in concentrations of Ca, Mg, K, and Na between groundwater, surface water, and snow in the two lakes. Lake B's groundwater generally showed higher concentrations of Ca, Mg, K, and Na than that of Lake A, suggesting that Lake B's groundwater may be more affected by water-rock interactions. Fig. 8 shows differences in concentrations of trace elements (Si, Li, Sr, Mn, Zn, and Cu) in groundwater, surface water, and snow in the two lakes. Lake B's groundwater showed a relatively higher concentration of Li, Sr, and Mn concentrations than that of Lake A, while Lake A's groundwater showed higher concentrations of Si, Zn, and Cu. This suggests that groundwater composition is dependent on both the type and degree of water-rock interaction, which is ultimately derived from chemical weathering of rocks (Vašinka et al., 2020).

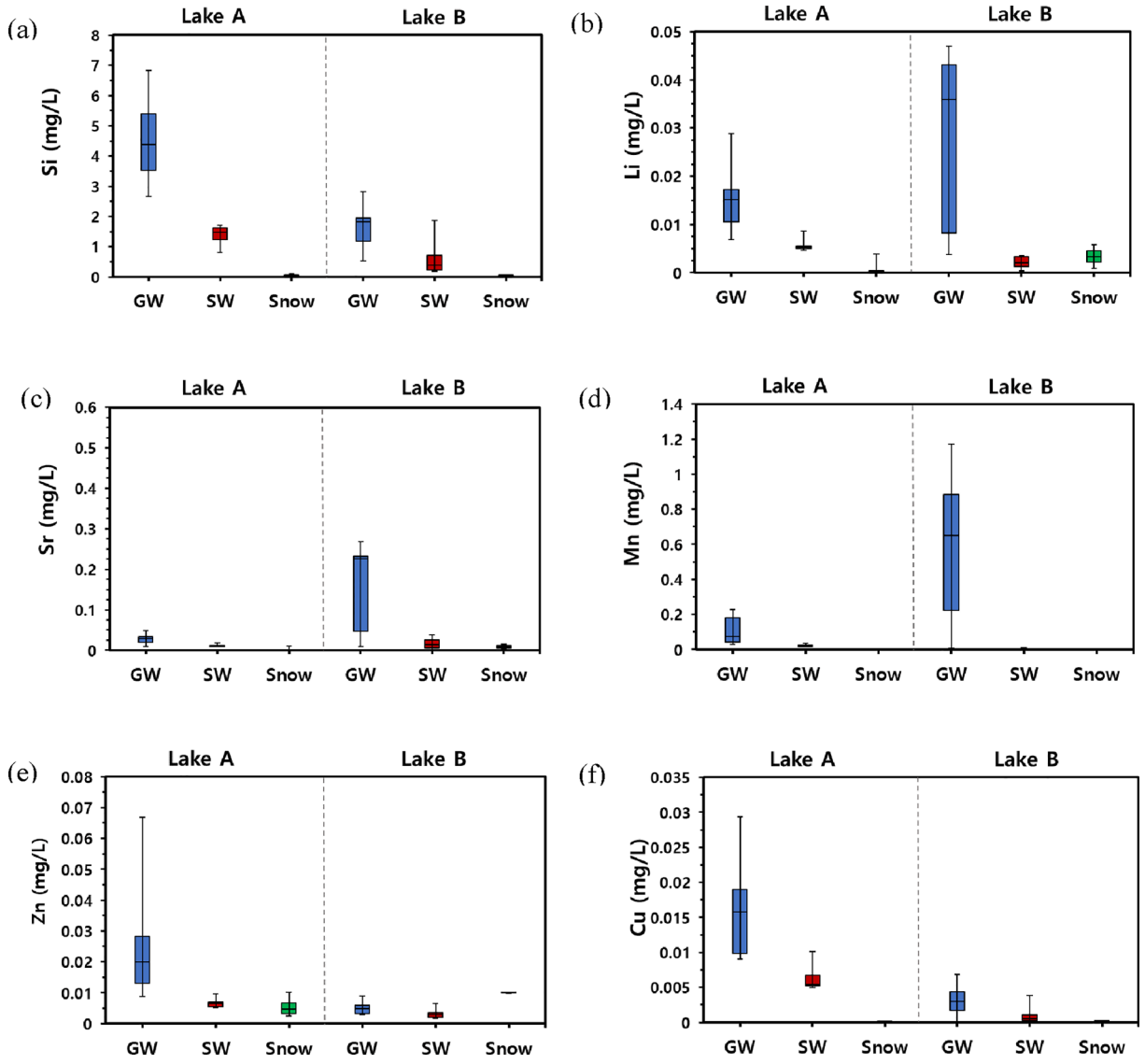

Fig. 8. Box and whisker plots showing distribution of trace elements ((a) Si, (b) Li, (c) Sr, (d) Mn, (e) Zn, and (f) Cu) in groundwater, surface water and snow of Lake A and Lake B. In the box plot, the center line represents the median, while the upper and lower lines represent the 75th and 25th percentiles, respectively. The upper and lower whiskers represent the maximum and minimum, respectively.

Overall, the water chemistry data confirm the flow systems of each lake that were identified by measuring groundwater fluxes and the water levels. To sum up, Lake A is a system where groundwater and surface water interact dynamically; groundwater quality is also affected by surface water and water qualities both for groundwater and surface water are thus fairly similar. Groundwater flows through the active layer and may be converted to interflow and overland flow while travelling to the lake. The size and volume of the lake are highly dependent on snow melt and precipitation. By contrast, Lake B is a stable system in which groundwater flows into surface water consistently. The groundwater flowing into Lake B has greater time to interact with aquifer materials, and thus shows higher concentrations of dissolved ions than Lake A.

5. Conclusions

This study evaluated the hydrogeological characteristics and interactions of groundwater, surface water, and snow in two lakes on the Barton Peninsula, Antarctica (referred to as “Lake A” and “Lake B” in this study). In particular, the flux of groundwater was measured to evaluate its role in two lake systems with different geological characteristics. In addition, hydraulic conductivity was calculated through grain size analysis of the lake sediments.

Whereas groundwater flux for Lake A showed dynamic changes, Lake B showed stable groundwater influx. The groundwater fluxes measured in Lake A were $-9.9 \times 10^{-10} \sim 2.7 \times 10^{-9}$ m/s (average of $-9.1 \times 10^{-10} \pm 3.6 \times 10^{-9}$ m/s), and in Lake B $2.2 \times 10^{-9} \sim 3.0 \times 10^{-9}$ m/s (average of $2.6 \times 10^{-9} \pm 4.0 \times 10^{-10}$ m/s). The dynamic changes in groundwater flux observed in Lake A indicate that it is a highly dynamic system, whereas the continued groundwater influx into Lake B allows the lake volume to remain relatively stable. Lake A and Lake B were composed of poorly sorted fine sand and coarse sand, respectively, and grain size and sorting correlated with the hydraulic conductivity values calculated. Hydraulic conductivity for the lake sediments ranged between 1.7×10^{-6} m/s and 2.1×10^{-4} m/s. The groundwater flux measured in the two lakes and the hydraulic conductivity of their sediments were not directly related to one another. This may be partly due to heterogeneity and uncertainty associated with the calculation of hydraulic conductivity through empirical formulae. In addition, uncertainties in measuring groundwater flux may be related to spatio-temporal variation. The flow characteristics of the lakes’ groundwater

systems appear to be influenced by the hydraulic gradient of each, which is governed by topography.

The water chemistry data support the interpretation for the hydrologic characteristics of each lake that were identified by measuring groundwater fluxes and the water levels. In Lake A, groundwater and surface water interacted dynamically, and thus water qualities both for groundwater and surface water were fairly similar. In contrast, surface water and groundwater in Lake B showed distinct geochemical characteristics. Groundwater composition was largely affected by water-rock interactions. Groundwater types in the study site were classified as Ca-HCO_3 and Ca-Na-SO_4-Cl, which were distinguishable from those of surface water and snow. The water quality type of snow belonged mainly to the Ca-Na-Cl and Na-Cl types, suggesting that snow composition may be affected by sea salt spray. Oxygen and hydrogen isotopic composition was generally consistent with the global meteoric water line (GMWL) and local meteoric water line (LMWL), indicating that groundwater and surface water in the study area originated from the atmosphere. Evaporation appears to be not a significant contributor to the lake hydrologic budgets, probably due to the relatively humid climate during the summer season. Both groundwater and surface water might partially experience isotopic fractionation during and after the snow melting process.

In summary, Lake A appears to be one of the small lakes of the polar region, its size and volume highly dependent on snow melt and precipitation. On the other hand, Lake B is largely maintained by groundwater infiltration, supplied by meltwater from the large amount of snow on the mountain slope. Overall, this study can be served as a basis for studying the role of groundwater in lake ecosystems in Antarctica and the impacts of climate change on the Antarctic water cycle. Groundwater fluxes into/out of the lake systems could be more dynamic considering the changes in depth and heterogeneity of the active layer in response to the seasonal variation in snow depth and melting rate. The basic information provided in this study and further investigation regarding the above issues can be used to construct quantitative evaluation tools, such as groundwater-surface integrated hydrogeologic models, to quantify the groundwater-surface water-snow/glacier interaction of the entire peninsula. Further studies necessary in this area include, while not being limited to, hydraulic head difference between groundwater and surface water, lake discharge rate, changes in the active layer and permafrost, and the mechanisms controlling water chemistry. A longer-term (e.g., year-round) monitoring should be considered to have a better understanding of the lake systems.

CRediT authorship contribution statement

Jisun Kim: Methodology, Data curation, Investigation, Writing - original draft, Visualization. **Sung-Wook Jeen:** Conceptualization, Formal analysis, Supervision, Project administration, Funding acquisition. **Hyoun Soo Lim:** Investigation, Resources. **Jeonghoon Lee:** Investigation, Resources. **Ok-Sun Kim:** Investigation, Resources, Data curation. **Hyoungseok Lee:** Resources, Data curation, Funding acquisition. **Soon Gyu Hong:** Resources, Supervision, Project administration.

Declaration of Competing Interest

The authors declare that they have no known competing financial interests or personal relationships that could have appeared to influence the work reported in this paper.

Acknowledgments

This research was supported by the Korea Polar Research Institute (PE20170) and the Polar Academic Program (PE20900) of the Korea Polar Research Institute. We appreciate Songyi Kim for water isotopes analysis. We would also like to thank the Writing Center at Jeonbuk National University for their language assistance.

Appendix A. Supplementary data

Supplementary data to this article can be found online at https://doi.org/10.1016/j.jhydrol.2020.125537.

References

Ahn, I.-Y., Lee, S.H., Kim, K.T., Shim, J.H., Kim, D.-Y., 1996. Baseline heavy metal concentrations in the Antarctic clam, Laternula elliptica in Maxwell Bay, King George Island, Antarctica. Mar. Pollut. Bull. 32 (8-9), 592–598.
Appello, C.A., Postma, D., 2005. Geochemistry, Groundwater and Pollution, 2nd ed. Balkema Publisher, Amsterdam.
Beyer, W., 1966. Hydrogeological investigations in the deposition of water pollutants. J. App. Geol. 12 (1), 599–606.
Bialas, Z., 1966. O usrednianiu wspolczynnikow filtracji z zastosowaniem elektronicznej cyfrowej maszyny matematycznej [Averaging filter coefficients using digital electronic mathematical machines]. Przedsiebiorstwo Geologiczne we Wroclawiu, Warsaw, Poland, pp. 47–50.
Carman, P.C., 1956. Flow of Gases Through Porous Media. Academic Press Incorporated, NY.
Carrier III, W.D., 2003. Goodbye, Hazen; Hello, Kozeny-Carman. J. Geotech. Geoenviron. Eng. 129 (11), 1054–1056.
Cheng, C., Chen, X., 2007. Evaluation of methods for determination of hydraulic properties in an aquifer–aquitard system hydrologically connected to a river. Hydrogeol. J. 15 (4), 669–678.
Cho, S.M., Lee, H., Hong, S.G., Lee, J., 2020. Study of ecophysiological responses of the Antarctic fruticose lichen Cladonia borealis using the PAM fluorescence system under natural and laboratory conditions. Plants 9 (1), 85.
Chun, H.Y., Chang, S.K., Lee, J.I., 1994. Biostratigraphic study on the plant fossils from the Barton Peninsula and adjacent areas (in Korean with English abstract). J. Paleontol Soc. Korea 10, 69–84.
Craig, H., 1961. Isotopic variations in meteoric waters. Science 133 (3465), 1702–1703.
Ducklow, H.W., Baker, K., Martinson, D.G., Quetin, L.B., Ross, R.M., Smith, R.C., Stammerjohn, S.E., Vernet, M., Fraser, W., 2007. Marine pelagic ecosystems: the West Antarctic Peninsula. Phil. Trans. R. Soc. B 362 (1477), 67–94.
Fernandoy, F., Meyer, H., Tonelli, M., 2012. Stable water isotopes of precipitation and firn cores from the northern Antarctic Peninsula region as a proxy for climate reconstruction. Cryosphere 6, 313–330.
Fetter, C.W., 1994. Applied Hydrogeology Third Edition University of Wisconsin-Oshkosh. Mc Millian College Publishing Company, New York.
Folk, R.L., 1954. The distinction between grain size and mineral composition in sedimentary-rock nomenclature. J. Geol. 62 (4), 344–359.
Folk, R.L., Ward, W.C., 1957. Brazos River bar [Texas]; a study in the significance of grain size parameters. J. Sediment. Res. 27 (1), 3–26.
Hazen, A., 1892. Some Physical properties of sands and gravels, with special reference to their use in filtration. 24th Ann. Rept., Mass. State Board of Health Pub. Doc. 34, 539–556.
Headland, R.K., 1984. The Island of South Georgia. Cambridge University Press, Cambridge, UK, Cambridge.
Healy, R.W., Scanlon, B.R. (Eds.), 2010. Estimating Groundwater Recharge. Cambridge University Press, Cambridge.
Hofstee, E.H., Campbell, D.I., Balks, M.R., Aislabie, J., 2006. Groundwater characteristics at Seabee Hook, Cape Hallett, Antarctica. Antartic Sci. 18 (4), 487–495.
IPCC, W., Davidson, O., Swart, R., Pan, J., 2001. Climate change 2001: mitigation. contribution of working group III to the third assessment report of the intergovernmental panel on climate change. Cambridge University Press, Cambridge, UK.
Jeong, G.Y., Yoon, H.I., 2001. The Origin of Clay Minerals in Soils of King George Island, South Shetland Islands, West Antarctica, and its implications for the clay-mineral compositions of marine sediments. J. Sediment. Res. 71 (5), 833–842.
Jeong, Gi Young, Yoon, Ho Il, Lee, Seung Yeop, 2004. Chemistry and microstructures of clay particles in smectite-rich shelf sediments, South Shetland Islands, Antarctica. Mar. Geol. 209 (1-4), 19–30.
Jung, Youn-Young, Koh, Dong-Chan, Lee, Jeonghoon, Ko, Kyung-Seok, 2013. Applications of Isotope Ratio Infrared Spectroscopy (IRIS) to Analysis of Stable Isotopic Compositions of Liquid Water동위원소비 적외선 분광법(IRIS)을 이용한 물 안정동위원소 분석. Econ. Environ. Geol. 46 (6), 495–508.
Kasenow, M., 2002. Determination of Hydraulic Conductivity from Grain Size Analysis. Water Resour. Pub, Littleton, Colorado.
Khim, Boo-Keun, Park, Byong-Kwon, Yoon, Ho Il, 1997. Oxygen isotopic compositions of seawater in the Maxwell Bay of King George Island, West Antarctica. Geosci J 1 (2), 115–121.
Kim, Intae, Kim, Guebuem, Choy, Eun Jung, 2015. The significant inputs of trace elements and rare earth elements from melting glaciers in Antarctic coastal waters. Polar Res. 34 (1), 24289. https://doi.org/10.3402/polar.v34.24289.
Kim, J.H., Ahn, I.Y., Lee, K.S., Chung, H., Choi, H.G., 2007. Vegetation of Barton Peninsula in the neighborhood of King Sejong Station (King George Island, maritime Antarctic). Polar Biol. 30 (7), 903–916.
Kim, M., Lee, I., Lee, J., Park, B., Mayer, B., Kaufman, A.J., Lee, K., 2008. Sulfur and oxygen isotopic composition of sulfate in the fresh water, King Sejong Station, King George Island, Antarctica. In AGU Fall Meeting Abstracts.

Kim, Taewan, Lee, Jeongsoon, Lim, Jeong Sik, 2019. Multipoint normalization of $\delta^{18}O$ of water against the VSMOW2-SLAP2 scale with an uncertainty assessment. Talanta 201, 379–387.
Knap, Wouter H., Oerlemans, Johannes, Cabée, Martin, 1996. Climate sensitivity of the ice cap of King George Island, South Shetland Islands, Antarctica. Ann. Glaciol. 23, 154–159.
Kwon, Tae-Yong, Lee, Bang-Yong, 2002. Precipitation Anomalies Around King Sejong Station, Antarctica Associated with E1Niño/Southern Oscillation. Ocean Polar Res. 24 (1), 19–31.
Lee, David R., Cherry, John A., 1979. A field exercise on groundwater flow using seepage meters and mini-piezometers. J. Geol. Educ. 27 (1), 6–10.
Lee, Jeonghoon, Feng, Xiahong, Posmentier, Eric S., Faiia, Anthony M., Taylor, Susan, 2009. Stable isotopic exchange rate constant between snow and liquid water. Chem. Geol. 260 (1-2), 57–62.
Lee, Jeonghoon, Hur, Soon Do, Lim, Hyoun Soo, Jung, Hyejung, 2020. Isotopic characteristics of snow and its meltwater over the Barton Peninsula, Antarctica. Cold Reg. Sci. Technol. 173, 102997. https://doi.org/10.1016/j.coldregions.2020.102997.
Lee, Jin-Yong, Lim, Hyoun Soo, Yoon, Ho Il, 2016. Thermal characteristics of soil and water during summer at King Sejong Station, King George Island, Antarctica. Geosci J 20 (4), 503–516.
Lee, Y.I., Choi, T., Lim, H.S., 2019. Petrological and geochemical compositions of beach sands of the Barton and Weaver peninsulas of King George Islands, West Antarctica: implications for provenance and depositional history. Episodes 42 (2), 149–164.
Lee, Yong Il, Lim, Hyoun Soo, Yoon, Ho Il, 2004. Geochemistry of soils of King George Island, South Shetland Islands, West Antarctica: implications for pedogenesis in cold polar regions. Geochim. Cosmochim. Acta 68 (21), 4319–4333.
Levy, Joseph, 2012. Hydrological characteristics of recurrent slope lineae on Mars: evidence for liquid flow through regolith and comparisons with Antarctic terrestrial analogs. Icarus 219 (1), 1–4.
Levy, J.S., Fountain, A.G., Gooseff, M.N., Welch, K.A., Lyons, W.B., 2011. Water tracks and permafrost in Taylor Valley, Antarctica: Extensive and shallow groundwater connectivity in a cold desert ecosystem. Geol. Soc. Am. Bull. 123, 2295–2311.
Lim, Hyoun Soo, Park, Youngyun, Lee, Jin-Yong, Yoon, Ho Il, 2014. Geochemical characteristics of meltwater and pondwater on Barton and Weaver Peninsulas of King George Island, West Antarctica. Geochem. J. 48 (4), 409–422.
Malandrino, Mery, Abollino, Ornella, Buoso, Sandro, Casalino, Claudia Elena, Gasparon, Massimo, Giacomino, Agnese, La Gioia, Carmela, Mentasti, Edoardo, 2009. Geochemical characterisation of Antarctic soils and lacustrine sediments from Terra Nova Bay. Microchem. J. 92 (1), 21–31.
Odong, J., 2013. Evaluation of empirical formulae for determination of hydraulic conductivity based on grain-size analysis. Int. J. Agric. Environ. 1, 1–8.
Park, Byong-Kwon, Chang, Soon-Keun, Yoon, Ho Il, Chung, Hosung, 1998. Recent retreat of ice cliffs, King George Island, South Shetland Islands, Antarctic Peninsula. A. Glaciology. 27, 633–635.
Quinton, W.L., Hayashi, M., Chasmer, L.E., 2011. Permafrost-thaw-induced land-cover change in the Canadian subarctic: implications for water resources. Hydrol. Process. 25 (1), 152–158.
Ross, R.M., Hofmann, E.E., Quetin, L.B., 1996. Foundations for Ecological Research West of the Antarctic Peninsula, vol. 70 American Geophysical Union, Washington, D.C.
Sawagaki, T., Hirakawa, K., 2002. Hydrostatic investigations on subglacial meltwater: implications for the formation of streamlined bedforms and subglacial lakes, East Antarctica. Polar Geosci. 15, 123–147.
Schiedek, Doris, Sundelin, Brita, Readman, James W., Macdonald, Robie W., 2007. Interactions between climate change and contaminants. Mar. Pollut. Bull. 54 (12), 1845–1856.
Schmidt, Logan M., Levy, Joseph S., 2017. Hydraulic conductivity of active layer soils in the McMurdo Dry Valleys, Antarctica: geological legacy controls modern hillslope connectivity. Geomorphology 283, 61–71.
Shepherd, Russell G., 1989. Correlations of Permeability and Grain Size. Ground Water 27 (5), 633–638.
Simões, J.C., Ferron, F.A., Bernardo, R.T., Aristarain, A.J., Stievenard, M., Pourchet, M., Delmas, R.J., 2004. Ice core study from the King George Island, South Shetlands, Antarctica. Pesqui. Antart. Bras. 4, 9–23.
Slichter, C.S., 1898. Theoretical investigations of the motion of ground waters. The 19th Ann. Rep. US Geophys. Survey 295–384.
Smith, Raymond, Baker, Karen, Fraser, William, Hofmann, Eileen, Karl, David, Klink, John, Quentin, Langdon, Prezelin, Barbara, Ross, Robin, Trivelpiece, Wayne, Vernet, Maria, 1995. The Palmer LTER: a long-term ecological research program at Palmer Station, Antarctica. oceanog 8 (3), 77–86.
Terzaghi, K., 1925. Principles of soil mechanics. Eng. News-Rec. 95, 832–836.
Uemura, Takeshi, Taniguchi, Makoto, Shibuya, Kazuo, 2011. Submarine groundwater discharge in Lützow-Holm Bay, Antarctica: SGD IN ANTARCTICA. Geophys. Res. Lett. 38 (8), n/a–n/a.
Vašinka, Martin, Krmíček, Lukáš, Všianský, Dalibor, Hrbáček, Filip, Nývlt, Daniel, 2020. Chemical weathering in Antarctica: an example of igneous rock particles in Big Lachman Lake sediments, James Ross Island. Environ. Earth. Sci. 79 (8). https://doi.org/10.1007/s12665-020-08926-3.
Vukovic, M., Soro, A., 1992. Determination of Hydraulic Conductivity of Porous Media from Grain-Size Composition. Water Resources Publications, Littleton, Colorado.
Wentworth, Chester K., 1922. A scale of grade and class terms for clastic sediments. J. Geol. 30 (5), 377–392.
Wingham, Duncan J., Siegert, Martin J., Shepherd, Andrew, Muir, Alan S., 2006. Rapid discharge connects Antarctic subglacial lakes. Nature 440 (7087), 1033–1036.
Yeo, Jeong Pil, Lee, Jong Ik, Hur, Soon Do, Choi, Byeon-Gak, 2004. Geochemistry of volcanic rocks in Barton and Weaver peninsulas, King George Island, Antarctica: implications for arc maturity and correlation with fossilized volcanic centers. Geosci. J. 8 (1), 11–25.
Yoo, C.M., Choe, M.Y., Jo, H.R., Kim, Y., Kim, K.H., 2001. Volcaniclastic sedimentation of the Sejong Formation (Late Paleocene-Eocene), Barton Peninsula, King George Island, Antarctica (in Korean with English abstract). Ocean Polar Res. 23 (2), 97–107.